

1 **Modeling the optical spectra of supported nanoparticle ensembles:**
2 **Extraction of the relationship between particle shape and size**

3
4 C. Hendrich¹, T. Vartanyan, F. Hubenthal, and F. Träger

5
6 Institut für Physik

7 and

8 Center for Interdisciplinary Nanostructure Science and Technology – CINSaT,

9 Universität Kassel, Heinrich-Plett-Strasse 40, 34132 Kassel, Germany

10
11 ¹ Present address: Carl Zeiss NTS GmbH, Carl-Zeiss-Straße 56, 73447 Oberkochen, email:
12 christian@hendrich.org

13
14
15 **Abstract**

16 A new method for modeling the extinction spectra of metal nanoparticle ensembles with a
17 broad size and shape distribution is presented. The technique is based on fitting the results of
18 calculations in quasistatic approximation to the inhomogeneously broadened extinction
19 profile of the nanoparticles. As result a distribution of the particle axial ratios and furthermore
20 the relationship between axial ratio and radius of particles within the ensemble are
21 determined.

22 Our technique can be applied to oblate nanoparticles which exhibit a strong correlation
23 between the shape and size of the particles, e.g. to supported nanoparticles which are
24 generated by deposition of atoms and subsequent nucleation, i.e. by Volmer-Weber-growth.
25 As example we applied the method to gold and silver nanoparticles on sapphire and TiO₂
26 surfaces and found a perfect agreement between the calculated and experimental data.
27 Furthermore, the extinction spectra of particle ensembles irradiated with nanosecond laser
28 pulses during and after growth were modeled. Our technique not only allows us to reproduce
29 the experimental data but also reveals important and new information about the morphology
30 of the nanoparticle ensembles, even the changes of the average particle radius and the amount
31 of desorbed atoms after laser interaction, which otherwise cannot be obtained. The results
32 show the successful reshaping of resonant nanoparticles by selective laser-heating of the
33 particles. The average particle radius after laser interaction was successfully calculated from
34 the optical spectra.

1 **1. Introduction**

2 The optical response of small metal nanoparticles is dominated by an excitation of a surface
3 plasmon-polariton resonance which is the result of a collective oscillation of the conduction
4 band electrons in the nanoparticles [Mie08, Bohren83, Kreibig95]. The surface plasmon-
5 polariton, in this paper shortly denoted as plasmon, is supposed to play an important role for
6 many future applications such as optical waveguides [Maier03], surface enhanced Raman
7 scattering [Mandal04], Biosensors [Heas04, Raschke03] or as markers for proteins [Bauer99].
8 Nevertheless, the energetic position of the plasmon resonance in the optical spectrum is
9 considerably affected by the nanoparticle material, size, shape and the dielectric properties of
10 the surrounding material [Kreibig95]. Thus, a precise analysis of the optical spectra can reveal
11 important structural information of the sample.

12 Since the determination of the morphology of nanoparticle ensembles is an important issue,
13 transmission electron microscopy (TEM) and scanning probe microscopy (SPM) are widely
14 used to investigate the size and shape of those particles. However, TEM and SPM allow in
15 most cases only ex-situ measurements and have several disadvantages: With TEM only thin
16 substrates can be investigated or the substrate has to be replaced by TEM grids. Furthermore,
17 in order to extract of the exact dimensions of the particles and to determine the size and axial-
18 ratio distributions by TEM, it has to be performed parallel and perpendicular to the substrate
19 surface or by using special substrates [Pauwels00]. Also a certain number of TEM
20 measurements are necessary to provide enough statistical data to extract the dependence of the
21 axial ratios on the equivalent radii or the axial ratio distributions of the nanoparticle
22 ensembles

23 In general, SPM can only be applied to (immobilized) nanoparticles on surfaces and usually
24 the convolution of the nanoparticle shape by that of the probe tip makes the determination of
25 the exact dimensions impossible. Moreover, SPM and TEM are limited to small sections of
26 the samples and the collected data is neither sufficient for statistical evaluation nor represents
27 the sample structure on larger scales. An alternative and adjuvant tool is the optical
28 characterization with extinction spectroscopy [Germain05, Xu05, Rentiera05, Wenzel99,
29 Stietz01] which is non-destructive and can be used in situ.

30 However, optical characterization is usually not a straightforward method since most
31 nanoparticle ensembles exhibit non-uniform optical properties due to size and shape
32 distributions [Fedotov04, Burshtain99, Fu05, Stietz01]. This leads to an inhomogeneous
33 broadening of the plasmon resonance which has to be taken into account if the experimental
34 data is modeled. Also the influence of the particle surrounding, e.g. of the underlying

1 substrate, and the interaction among the particles has an influence of the optical properties
2 [Kreibig95, Yamaguchi74]. The latter effect can be neglected as long as the inter-particle
3 distances are large or particles with an equal plasmon frequency are not close to each other
4 [Kreibig85]. For these reasons the determination of the radii and the axial ratios of each single
5 nanoparticle in the distribution by the evaluation of the optical spectra of nanoparticle
6 ensembles is a complicated task, but the results reveal important information of the particle
7 dimensions.

8 The considerations above show that no single experimental technique available today can
9 directly provide reliable data on the size and shape distributions of ensembles of supported
10 metal nanoparticles. In this contribution we are going to present a new model that combines
11 the results of several experimental techniques in such a way that useful estimations of the
12 correlation between the size and shape distributions of the nanoparticles become readily
13 obtainable. The proposed method can reproduce the absorption and extinction spectra of the
14 particle ensembles and extracts the functional dependence of the shape and size of the
15 nanoparticles, only by using the known properties of the systems under study.

16 Our model may be applied to the experimental data of several measurements [Xu05,
17 Germain05, Renteria05, Ouacha05, Wenzel99, Stietz01] where the full potential of the
18 evaluation of the absorption and extinction spectra was not exploited. It can also be used to
19 obtain precise information about the morphology of nanoparticle ensembles which have been
20 exposed to laser irradiation either during or after nanoparticle growth, e.g. for laser assisted
21 growth [Wenzel99a, Bosbach00, Ouacha05, Link00, Safonov98, MacDonald02], or the
22 spectral hole burning technique [Bosbach02, Hendrich03, Ziegler04]. In such experiments,
23 the radius of the particles whose axial ratio is to be altered by laser irradiation is initially
24 unknown. The radius can henceforth be calculated with the model presented in this
25 publication which was already used for size-dependent investigations of the dephasing time
26 [Bosbach02, Hendrich03, Ziegler04]. Moreover, since the interaction with the laser light also
27 induces desorption and diffusion, our technique can be used to calculate the remaining
28 coverage on the substrate and the average radius of the modified nanoparticles.

29 After a short experimental section we will first describe our method in detail and afterwards
30 apply it to the experimental data obtained from different nanoparticle ensembles.

31

32 **2. Experimental**

33 The nanoparticles were prepared under ultrahigh vacuum conditions by Volmer-Weber
34 growth, i.e. by deposition of gold and silver atoms on sapphire and TiO₂ surfaces followed by

1 diffusion and nucleation. The surface coverage was measured by a quartz crystal flux monitor.
2 The generated particles could be approximated by oblate rotational ellipsoids and exhibited
3 broad size and shape distributions [Stietz01]. Most important, the shape of the particles is
4 determined by the surface energy of the particles and the substrate and thus depends explicitly
5 on the particle size [Winterbottom67].

6 After preparation, AFM was employed to determine the number density of the nanoparticles
7 on the substrate. Assuming bulk properties of the nanoparticles, the average particle volume
8 was calculated from the amount of deposited material and the number density of the
9 nanoparticles on the surface [Wenzel99]. For the characterization of the nanoparticles the
10 equivalent radius R_{eq} was used. It corresponds to the radius of a sphere with the same volume
11 as the actual ellipsoid and is determined by

$$12 \quad V = \frac{4}{3} \pi R_{eq}^3 . \quad (1)$$

13 Although the direct determination of the nanoparticle size and shape was not possible with
14 AFM, the relative size distribution of the particles can be reproduced correctly as long as the
15 mapped dimensions are enlarged by the AFM tip linearly [Grabar97].

16 The optical spectra of the particles were measured in situ using the light of a xenon arc lamp
17 in combination with a monochromator. The samples were illuminated under an angle of
18 incidence of 45° with respect to the surface normal using s- or p-polarized light with photon
19 energies between 1.3 – 4.5 eV (276 – 954 nm). The transmitted light was detected by a
20 photodiode and compared with a reference signal recorded in front of the sample.

21 For laser treatment, a BBO-OPO (beta-barium-borate optical parametric oscillator) was used
22 which was pumped by the third harmonic of a Nd:YAG laser. The pulse duration was about
23 5.5 ns at a repetition rate of 10 Hz. The laser beam diameter on the sample was (2 ± 0.15)
24 mm.

25 26 **3. Modeling the extinction spectra**

27 We use the following assumptions and simplifications for our model.

- 28 1. The calculation of the optical spectra by the so-called quasistatic approximation is
29 sufficient which assumes that the particles are small compared to the wavelength of
30 the light, i.e. the electromagnetic field within the particles is spatially nearly constant
31 [Bohren83, Kreibig95]. As a result, the size, or more precisely, the volume of the
32 particles only affects the amplitude of the plasmon resonances, but not their spectral
33 positions. Therefore, in the size range from 1 nm to 20 nm the calculated spectral

1 positions of the plasmon resonances are definitely determined by the axial ratio $x =$
2 a/b of the particles [Bohren83].

- 3
- 4 2. The particles are approximated by ellipsoidal nanoparticles with a Gaussian size
5 distribution which is usually fulfilled for particles grown on surfaces or deposited
6 from a gas phase [Wenzel99, Xu05, Bowen99]. The optical spectra of the ellipsoids
7 are dominated by two plasmon modes. The (1,0)-mode which corresponds to an
8 excitation of the electrons along the short axis a of the particle and the (1,1)-mode to
9 an excitation along the long axis b , i.e. perpendicular and parallel to the substrate,
10 respectively [Bohren83]. Depending on the nanoparticle material, polarization and
11 incident angle of the light which were used as input parameters for the model, either
12 one or both plasmon modes show up in the optical spectrum of the ellipsoids.
- 13
- 14 3. In the calculations, we employ the optical properties of the bulk materials without any
15 modifications (e.g. from [Grigoriev97]). Although it is not strictly correct, recent
16 observations prove that major disagreements may be anticipated for particles smaller
17 than 1 nm or larger than 20 nm [Kreibig95]. Therefore our technique is intended to
18 deal with larger particles.
- 19
- 20 4. The influence of the substrate on the plasmon resonance was included by the effective
21 medium theory [Kreibig95]. In this approximation an average dielectric function of
22 the particle surrounding is used, calculated by using a mixing factor which is the
23 fraction of the particle surface in contact to the substrate. The mixing factor can be, for
24 example, determined from the positions of the (1,0)- and the (1,1)-mode of the
25 plasmon [Wenzel99].
- 26
- 27 5. A strong correlation between size and shape of the nanoparticles is observed in several
28 experiments [Wenzel99]. This link between size and shape can be due to the growth
29 kinetics in Volmer-Weber-growth where small particles are nearly spherical and get
30 increasingly oblate as they become larger [Stietz01]. We translate this correlation into
31 the assumption of a one to one correspondence between size and shape. In this way,
32 the problem gets more tractable and the particle ensemble can be characterized by the
33 functional dependence of the shape and the size.
- 34

1 The modeling is performed in two steps. First, the distribution of the volume-weighted axial
 2 ratios of the particles is calculated by fitting the experimental data with a theoretically
 3 obtained spectrum. Second, we employ the fact that in most cases the shape of nanoparticles
 4 on surfaces is directly depending on their size. Providing the validity of this correlation and
 5 the number density of the nanoparticles on the surface which is determined experimentally by
 6 atomic force microscopy (AFM), we can finally attribute the axial ratio of a single particle in
 7 the ensemble to its radius and obtain this functional dependence.

8 For the first step, i.e. for modeling of the a/b -distribution, we only use the optical extinction
 9 spectra as input from the experiment (section 3.1). For the second step, i.e. the calculation of
 10 the dependence of the axial ratio on the particle size (section 3.2), we further supply the
 11 average equivalent radius of the particles, the width of their size distribution and the
 12 nanoparticle number density on the substrate. In the examples given in section 4 we also use
 13 the average equivalent radius as an additional free parameter in the fits.

14

15 **3.1. Determination of the apparent a/b -distribution**

16 In order to model the extinction spectra of the particle ensemble we need first the value of the
 17 absorption cross section of a single particle with a particular axial ratio x and volume V at a
 18 given frequency ω . According to [Bohren83] the spectrum in quasistatic approximation is
 19 given by

$$20 \quad s(\omega, x) = \frac{V\omega}{c} \operatorname{Im} \left\{ \frac{\varepsilon(\omega) - 1}{1 + [\varepsilon(\omega) - 1]L(x)} \right\}, \quad (2)$$

21 where $L(x)$ is the depolarization factor known for any axial ratio x , c is the speed of light and
 22 $\varepsilon(\omega) = \varepsilon_l(\omega)/\varepsilon_m$ with $\varepsilon_l(\omega)$ and ε_m being the dielectric permittivities of the particle material
 23 and the surrounding medium, respectively. Under our assumption of strong correlation
 24 between size and shape, the particle volume V is not an independent variable but rather a
 25 function of the axial ratio $V(x)$. If all particles were of the same size and shape, the extinction
 26 spectra could be obtained as a product of $s(x, \omega)$ and the surface number density of the
 27 particles n . To account for the actual size and shape distribution we introduce a probability
 28 distribution function $f_{ab}(x)$ which satisfies a normalization condition

$$29 \quad \int_0^1 f_{ab}(x) dx = 1. \quad (3)$$

30 The upper limit of integration corresponds to spherical particles and it is taken for granted that
 31 the particles with axial ratios larger than 1, that is, prolate particles, are not present on the
 32 surface [Wenzel99]. Then, the extinction spectrum of the particle ensemble is given by

$$1 \quad S_{ab}(\omega) = n \int_0^1 f_{ab}(x) s(x, \omega) dx. \quad (4)$$

2 Substituting $s(x, \omega)$ by Eq. (1) one finds

$$3 \quad S_{ab}(\omega) = \frac{n}{c} \int_0^1 f_{ab}(x) V(x) \omega \operatorname{Im} \left\{ \frac{\varepsilon(\omega) - 1}{1 + [\varepsilon(\omega) - 1] L(x)} \right\} dx. \quad (5)$$

4 Eq. (5) may be regarded as an integral equation for the product $f_{ab}(x)V(x)$. From the
5 mathematical point of view it is a Fredholm equation of the first kind which is known to be
6 ill-conditioned [Press92]. To get a reasonable solution, a proper regularization procedure
7 should be applied. In our case any measure of smoothness of the solution together with
8 constrain of positivity may be employed for the regularization.

9 An extremely simple solution may be obtained if the homogeneous broadening of the
10 plasmon resonance is much smaller than the width of the inhomogeneously broadened profile
11 of the nanoparticle ensemble. Let $x(\omega)$ be the axial ratio of the particle with resonance
12 frequency ω . In this case the imaginary part of the value in curl brackets in Eq. (5) is a
13 maximum at this particular value of x and dies away in its nearest neighborhood. The product
14 $f_{ab}(x)V(x)$, on the other hand, is almost constant in the region where the other term goes from
15 its maximum to almost zero. Hence, the product $f_{ab}(x)V(x)$ may be taken out of the integral at
16 $x = x(\omega)$ and the remaining part has to be integrated to give

$$17 \quad S_{ab}(\omega) = f_{ab}(x(\omega)) V(x(\omega)) \frac{\omega n}{c} \int_0^1 \operatorname{Im} \left\{ \frac{\varepsilon(\omega) - 1}{1 + [\varepsilon(\omega) - 1] L(x)} \right\} dx. \quad (6)$$

18 Hence,

$$19 \quad f_{ab}(x(\omega)) V(x(\omega)) = \frac{S_{ab}(\omega)}{\frac{n\omega}{c} \int_0^1 \operatorname{Im} \left\{ \frac{\varepsilon(\omega) - 1}{1 + [\varepsilon(\omega) - 1] L(x)} \right\} dx}. \quad (7)$$

20 Even when the homogeneous broadening of the plasmon resonance is not much smaller than
21 the width of the inhomogeneous broadening Eq. (7) may serve as a good starting point for the
22 numerical solution of the regularized Eq. (4).

23 Beginning with the result from Eq. (7), we replace $f_{ab}(x)V(x)$ in Eq. (5) by spline with about
24 ten to twenty sampling points and adapt it to the experimental data by minimizing the mean
25 error squares [Press92]. This method is unambiguously because the spectral position of the
26 plasmon resonance is linked to the axial ratio of the nanoparticles by a steady and monotonic
27 function, i.e. the imaginary part of Eq. (2) [Bohren83].

28 The resulting function for the product $f_{ab}(x)V(x)$ in Eq. (5) reflects the impact of the particles
29 with a certain axial ratio on the optical spectrum and is denoted in the following as *apparent*

1 *axial ratio distribution*. For example, the axial ratio where $f_{ab}(x)V(x)$ peaks is the axial ratio
 2 which corresponds to the centre frequency of the plasmon peak but is *not* the most probable
 3 axial ratio in the particle distribution which would be the maximum of the function $f_{ab}(x)$.
 4 However, the knowledge of the apparent axial ratio distribution is useful for many
 5 experiments because it reflects how strong particles with certain axial ratios contribute to the
 6 optical response of the nanoparticle ensemble.

7

8 **3.2. Determination of the relationship between radius and axial ratio of a single** 9 **nanoparticle**

10 In the apparent axial ratio distribution $f_{ab}(x)V(x)$, the axial ratio of the particles is still
 11 convoluted with their volume. In this section we will determine a function $x(R_{eq})$ which
 12 allows to attribute a certain axial ratio x to the radius R_{eq} of a defined single particle despite
 13 the apparent particle ensemble. The presented method will only work for nanoparticles where
 14 the axial ratio is strongly correlated to their size, e.g. for samples prepared by Volmer-Weber-
 15 growth where the shape of the particles is determined by the surface energies of the
 16 concurring materials [Bäumer99, Wakayama99, Wenzel99].

17 For the calculations the size distribution of the nanoparticle ensemble $f_R(R_{eq})$ that can be
 18 easily obtained by AFM is necessary as additional input. The size distribution $f_R(R_{eq})$ can be
 19 approximated as a Gaussian [Stietz01] with the average equivalent radius $\langle R_{eq} \rangle$ and the
 20 relative standard deviation σ_R . It has to satisfy the normalization condition

$$21 \int_0^{\infty} f_R(R_{eq}) dR_{eq} = 1. \quad (8)$$

22 We assume that $x(R_{eq})$ is a monotone and continuous function which means, that the axial
 23 ratio is depending explicitly on the radius. The relationship $x(R_{eq})$ is found by equating two
 24 forms of the same probability distribution

$$25 f_R(R_{eq}) dR_{eq} = -f_{ab}(x) dx. \quad (9)$$

26 The minus sign accounts for the fact that large particles have smaller axial ratio. Since optical
 27 spectroscopy provides only $f_{ab}(x)V(x)$ instead of $f_{ab}(x)$, Eq. (9) has to be multiplied by $V(x)$.

28 With Eq. (1) one finds

$$29 f_R(R_{eq}) \frac{4}{3} \pi R_{eq}^3 dR_{eq} = -f_{ab}(x) V(x) dx. \quad (10)$$

30 The integrand in Eq. (4) can be now rewritten as a function depending on R_{eq} and ω only. By
 31 introducing the function $x(R_{eq})$ we find for the optical spectrum of the particles

$$S_R(\omega) = \frac{n}{c} \int_0^\infty f_R(R_{eq}) \frac{4}{3} \pi R_{eq}^3 \omega \operatorname{Im} \left\{ \frac{\mathcal{E}(\omega) - 1}{1 + [\mathcal{E}(\omega) - 1] L(x(R_{eq}))} \right\} dR_{eq}. \quad (11)$$

Integrating both sides of Eq. (10) gives

$$\int_0^{R_{eq}} f_R(R'_{eq}) \frac{4}{3} \pi (R'_{eq})^3 dR'_{eq} = \int_x^1 f_{ab}(x') V(x') dx'. \quad (12)$$

The limits of the integration are chosen with the understanding that smaller particles are spherical while larger particles are oblate. The inverse order of the integration limits accounts for the minus sign in Eq. (10) and ensures that both sides of Eq. (12) are positive. Numerical integration readily provides both functions $x(R_{eq})$ and $R_{eq}(x)$.

Eq. (12) enables one to check if the optical data are in accord with the morphological data obtained by AFM. For a consistent set of data, Eq. (12) is expected to be valid also in the limit when $R_{eq} \rightarrow \infty$ and $x \rightarrow 0$. However, if the experimental data do not satisfy Eq. (12) in this limiting case one can consider an appropriate renormalization of the morphological data. This might be necessary, due to a reconsideration of the sticking coefficient on the surface, or a recalculation of the number density of the nanoparticles taking another convolution of the AFM-tip radius into account, or by re-evaluation of any other suspicious parameter involved in the determination of the real amount of the material present on the surface. Another source of discrepancy may be connected with the extinction measurements. In the present form the theory does not take into account reflection which may greatly modify extinction for dense samples [Bonch01]. In what follows we restrict the applications to cases of not too dense samples, in particular, extinction will never exceed 60%. Finally, if there is no definitive information about the amount of the material present on the surface Eq. (12) may be employed to get an estimate of it.

The calculated function $x(R_{eq})$ is very powerful as it permits one to determine the exact dimensions of the particles *within* the nanoparticle ensemble. Furthermore, $x(R_{eq})$ can be used as a basis for further models, e.g. theoretical considerations of laser interaction with a nanoparticle ensemble, as will be demonstrated in Sec. 4.4 and 4.5.

1 **4. Results**

2 **4.1. Silver nanoparticles on sapphire**

3 As a first proof of the accuracy of the new model, we analyzed an ensemble of oblate silver
4 nanoparticles on a sapphire substrate. From the AFM analysis we determined a nanoparticle
5 number density of $1.5 \cdot 10^{11} \text{ cm}^{-2}$, an average radius of $\langle R_{eq} \rangle = 8.3 \text{ nm}$ and a relative width of
6 the size distribution of about 34% (HWHM) for this sample. The extinction spectrum clearly
7 exhibits the (1,0)- and (1,1)-mode of the surface plasmon polariton (Fig. 1a and 1c, squares).
8 Since both plasmon peaks have to be fitted by the model, this data is a good benchmark to
9 demonstrate the functionality of our method. First, Eq. (5) was adapted to the extinction
10 spectrum by using quasistatic approximation with a mixing factor of 0.2 which was already
11 used in [Wenzel99] and the dielectric function of silver [Edward98]. Despite the difficulty to
12 fit both plasmon modes, the experimental data is excellently reproduced by Eq. (5) (Fig. 1a,
13 solid line). The values for the product $f_{ab}(x)V(x)$ obtained in this way are shown in the Fig. 1b.
14 We stress here that the value of $x = 0.21$ at which $f_{ab}(x)V(x)$ peaks is neither the most probable
15 axial ratio nor it is a mean axial ratio of the particle ensemble as it was often assumed earlier
16 [Wenzel99]. As compared to the true probability distribution of the axial ratios $f_{ab}(x)$, the
17 maximum of the curve in the Fig. 1b is shifted to smaller values because of the presence of
18 the additional multiplier $V(x)$ that takes into account the favoured absorption of larger
19 particles.

20 To extract the correlation between the axial ratio and equivalent radius Eq. (12) was solved
21 numerically. With this data, the spectrum can be calculated by Eq. (11). It is shown as solid
22 line in Fig. 1c and reproduces the experimental data very well, especially the two plasmon
23 peaks. The calculated function $x(R_{eq})$ is shown in Fig. 1d as a solid line. The function exhibits
24 a monotonous decrease from $x = 1$ for small particles down to $x = 0.1$ for large particles. Fig.
25 1d plots also the probability distribution of the equivalent radius as obtained from AFM in
26 arbitrary units (dotted line). The probability distribution for the axial ratio can now be easily
27 obtained either by dividing $f_{ab}(x)V(x)$ by $V(x)$, or by a direct transformation of probability
28 distributions according to Eq. (9)

$$29 \quad f_{ab}(x) = -f_R(R_{eq}) \frac{dR_{eq}}{dx} \quad . \quad (13)$$

30 Both ways lead to the same result for the axial ratio of the most probable radius that is also
31 shown in Fig. 1d by the dashed arrow. From this plot one finds that the most probable axial
32 ratio is $x = 0.49$ at the most probable equivalent radius of $R_{eq} = 8.3 \text{ nm}$.

1 We have to point out that the most probable equivalent radius and the most probable axial
2 ratio are not connected by the function $x(R_{eq})$. Indeed, differentiating Eq. (13) with respect to
3 x leads to

$$4 \quad \frac{df_{ab}(x)}{dx} = -\frac{df_R(R_{eq})}{dR_{eq}} \left(\frac{dR_{eq}}{dx} \right)^2 - f_R(R_{eq}) \frac{d^2 R_{eq}}{dx^2} \quad (14)$$

5 From Eq. (14) it is clear that the probability distributions of x and R_{eq} can reach their
6 respective maxima simultaneously ($df_{ab}(x)/dx = df_R(R_{eq})/dR_{eq} = 0$) only, if the last term in
7 Eq. (14) equals zero. However, in general this condition does not apply.

1 4.2. Silver nanoparticles on TiO₂

2 An absorption spectrum of silver nanoparticles which were grown onto a TiO₂ substrate by rf
3 magnetron sputtering by Xu et. al [Xu05] has been evaluated by using our model. First, we
4 calculated the average equivalent radius and the number density of the nanoparticles on the
5 surface from the top-view TEM image (Fig. 2b in [Xu05]) by using the amount of silver
6 deposited on the substrate of an equivalent thickness of 3.3 nm. As result we found a number
7 density of the nanoparticles of $8.9 \cdot 10^{10} \text{ cm}^{-2}$, a size distribution of 30% and $\langle R_{\text{eq},\text{Xu}} \rangle = 8.9$
8 nm. As input for our model we used the dielectric constant of the TiO₂ substrate of $\epsilon = 7.56$, a
9 mixing factor of 0.2 and the absorption spectrum recorded by Xu (Fig. 3 in [Xu05]) which
10 corresponds to the nanoparticle ensemble depicted in the TEM picture. In our model the angle
11 of incidence was set to 90° with respect to the surface normal, in accordance with the
12 experiment. Due to these settings the (1,0)-mode of the plasmon resonance can not be excited
13 and is not visible in the absorption spectrum. The experimental data and the fit by Eq. (5) are
14 plotted in Fig. 2a by squares and the solid line, respectively. The absorption spectrum is
15 nicely reproduced in the region of the plasmon peak. The resulting apparent axial ratio
16 distribution has a maximum at $x = 0.07$ (Fig. 2b).

17 In addition we used $\langle R_{\text{eq},\text{Xu}} \rangle = 8.9$ nm to model the absorption spectrum by Eq. (5) (Fig. 2c,
18 dashed line). As result, we found a significant deviation from the experimental spectrum which
19 we attribute to an overestimation of $\langle R_{\text{eq},\text{Xu}} \rangle$. Thus, we used $\langle R_{\text{eq}} \rangle$ as a free parameter in Eq.
20 (12) and varied it until we could reproduce the measured data with our model (Fig. 2c, solid
21 line). The best fit was obtained for $\langle R_{\text{eq}} \rangle = 6.9$ nm. The reason for this difference might be
22 that the adsorption coefficient of silver on the substrate was smaller than expected or the
23 silver flux was not constant during nanoparticle preparation. The radius distribution and the
24 resulting relationship between R_{eq} and x are plotted in Fig. 2d. The axial ratio at a radius of
25 $R_{\text{eq}} = \langle R_{\text{eq}} \rangle = 6.9$ nm has been determined to $x = 0.33$ by comparing $x(R_{\text{eq}})$ with the radius
26 distribution (Fig. 2d, dashed arrow). In order to compare these results to the data from the
27 TEM picture, we determined the lateral radius, i.e. the radius parallel to the long axis of the
28 particles. By using $x = 0.33$ and $R_{\text{eq}} = 6.9$ nm we calculated $\langle R_{\text{lateral}} \rangle = 10.0$ nm. This value is
29 in excellent agreement with the one we determined from the TEM picture from Xu which
30 amounts to $\langle R_{\text{lateral},\text{Xu}} \rangle = 10.2$ nm. This accordance between the two lateral radii of the
31 particles on the surface demonstrates the high accuracy of our model.

32
33

1 **4.3. Gold nanoparticles on sapphire**

2 As last example for non-irradiated nanoparticle ensembles, we evaluated an extinction
3 spectrum of gold nanoparticles on sapphire substrates in the same way as before. The
4 ensemble exhibits an average radius of $\langle R_{\text{eq}} \rangle = 6.3$ nm, $\sigma = 28$ % and a number density of
5 $3 \cdot 10^{11}$ cm⁻². In the extinction spectrum of the gold nanoparticles only the (1,1)-mode shows
6 up (Fig. 3a and 3c, squares), because the (1,0)-mode is damped due to the nearby interband
7 transition at 2.4 eV [Kreibig95, Johnson72]. For the calculation of the extinction spectra in
8 quasistatic approximation the dielectric function of gold [Johnson72] has been used. As
9 mixing factor 0.2 has been chosen which was calculated from the surface energies of the
10 metal and the substrate [Wakayama99, Bäumer99]. The results from fitting Eq. (5) and (12),
11 i.e. S_{ab} and S_{R} , respectively, to the experimental data are shown in Fig. 3a and 3c (solid lines).
12 Once again, perfect agreement is obtained. For this nanoparticle ensemble the axial ratio that
13 dominates in the optical spectrum, i.e. the maximum in the apparent axial ratio distribution is
14 $x = 0.16$ (Fig. 3b). Solving Eq. (12) and modeling the extinction spectra by use of Eq. (11)
15 reveals that the true average axial ratio of the particle ensemble is $x = 0.37$ and corresponds to
16 nanoparticles with $R_{\text{eq}} = \langle R_{\text{eq}} \rangle = 6.3$ nm (Fig. 3d, dashed line).

18 **4.4. Spectral hole burning**

19 To demonstrate the power of the model, we investigated also the extinction spectra of
20 nanoparticle ensembles after performing persistent spectral hole burning [Bosbach02,
21 Hendrich03, Ziegler04]. The ensemble of gold nanoparticles which has been already
22 investigated in the last section, was irradiated with laser light of a photon energy of 1.65 eV
23 (Fig. 4a, dashed line) and a laser fluence of (9.2 ± 0.5) mJ/cm². Fig. 4a depicts the extinction
24 spectra recorded before (squares) and after (open squares) laser irradiation. This data was
25 modeled by our method using the same parameters as in the last section (Fig. 4a, solid lines).
26 The resulting spectra are in good agreement with the experimental data despite the laser
27 induced modifications, showing the robustness of our model. For each case we determined the
28 apparent axial ratio distributions which are plotted in Fig. 4b. As a result of the laser treatment
29 the number of the particles with an axial ratio $x = 0.09$ is decreased while the number of
30 particles with a higher axial ratio of $x = 0.13$ is increased. The explanation for these changes
31 is that only the particles, whose plasmon is in resonance with the laser light (in our case
32 particles with $x = 0.09$) can absorb the energy from the laser pulses efficiently. They are
33 selectively heated and due to surface diffusion and desorption of atoms their shape is changed
34 towards more spherical and smaller particles [Vartanyan02, Vartanyan01, Bosbach02].

1 Finally, the relationship between axial ratio and particle radius (Fig. 3d) can be used to
2 determine the radius of the particles which are resonant with the laser light. In this case, for
3 nanoparticles with $x = 0.09$ it amounts to $R_{\text{eq}} = 8.9$ nm.

4 5 **4.5. Determination of $\langle R_{\text{eq}} \rangle$ after laser interaction**

6 Another important application of the model is to determine the average equivalent radius
7 $\langle R_{\text{eq}} \rangle$ of nanoparticle ensembles after laser interaction, i.e. experiments where the size and
8 shape of the particles has been modified by laser-induced desorption and diffusion [Stietz01,
9 MacDonald02]. In such experiments, the number of atoms left on the substrate is unknown
10 and the average equivalent radius $\langle R_{\text{eq}} \rangle$ of the nanoparticles cannot be determined. Once
11 again, our technique can solve this problem.

12 As example we examined an ensemble of gold nanoparticles on a sapphire substrate prepared
13 by laser assisted growth [Ouacha05, Wenzel99a, Bosbach00] where nanoparticle ensembles
14 with a predetermined axial ratio independent of the equivalent radius R_{eq} were produced. The
15 laser photon energy was chosen to be located at a lower energy compared to the plasmon
16 resonance of small particles. Since the axial ratio shrinks during growth, the plasmon
17 resonance shifts towards the photon energy of the laser light. As soon as the overlap of the
18 plasmon resonance and the laser line is large enough, the particles are selectively heated
19 [Vartanyan02], causing a competition of two processes: On the one hand the laser-induced
20 desorption and diffusion of atoms increases the axial ratio of the particles while on the other
21 hand the deposition of atoms decrease the axial ratio due to the growth kinetics. As a
22 consequence the shape, i.e. the axial ratio of the particles is kept constant despite the size of
23 the nanoparticles increases [Wenzel99a, Bosbach00, Ouacha05]. The application of our model
24 to such samples is possible because $x(R_{\text{eq}})$ is still a steady function with the special feature
25 that the axial ratio which is predetermined by the laser-assisted growth is now attributed to
26 several particle sizes.

27 The extinction spectrum of the investigated gold nanoparticle ensemble that was grown under
28 laser irradiation with a photon energy of 1.65 eV (vertical line in Fig. 5a and b) at a fluence of
29 (156 ± 16) mJ/cm² is shown in Fig. 5a (squares). In comparison to the spectrum of non-
30 irradiated gold nanoparticles (Fig. 3a), here the extinction for photon energies lower than the
31 laser photon energy is much smaller. It amounts to 10%, only, and is a result of the laser-
32 assisted growth. The spectrum modeled with Eq. (5) (Fig. 5a, solid line) agrees well with the
33 experimental data and also reproduces the abrupt decrease at about 1.65 eV. In the apparent
34 axial ratio distribution a sharp edge at the axial ratio which corresponds to the plasmon energy

1 of the particles that are resonant with the laser light is found (Fig. 5b). These results show that
2 on the sample surface nearly no particles with an axial ratio smaller than $x = 0.09$ exist which
3 demonstrates the efficiency of laser-assisted growth.

4 In the case of laser-assisted growth two effects have to be taken into account in order to
5 determine the average particle radius. First, the amount of material on the substrate is not
6 known, because the strong interaction of the laser light with the nanoparticles at high fluences
7 leads to desorption of atoms already mentioned before [Vartanyan02]. Second, the heating of
8 the substrate leads to coalescence of nanoparticles, i.e. their number density is smaller and
9 their average radius is larger compared to naturally grown nanoparticles [Wenzel99a,
10 Ouacha05]. The number density of the nanoparticles can be measured by AFM, but the
11 amount of the remaining material and thus, the average equivalent nanoparticle radius is
12 unknown. A solution for this lack of information is the usage of Eq. (12) to determine $\langle R_{eq} \rangle$.
13 The dashed line in Fig. 5a shows the calculated spectrum using the *uncorrected* amount of
14 material deposited on the surface which slightly overestimates the experimental data. Using
15 the equivalent particle radius as an additional free parameter as in section 4.2, Eq. (12) can be
16 nicely fitted to the experimental extinction data (Fig. 5a, solid line) if a value of $\langle R_{eq} \rangle = 17.4$
17 nm is used. With this value and the known number density of nanoparticles the amount of the
18 remaining material can be calculated. It amounts to $(87.8 \pm 9) \%$ in comparison to the amount
19 recorded during deposition by means of a quartz micro balance.

20 Since desorption of atoms from the nanoparticle surface depends strongly on the laser-
21 induced heating, a dependence on the laser fluence has been found (Fig. 6). For laser fluences
22 above 75 mJ/cm^2 a significant drop of the sticking coefficient is observed and finally an
23 effective sticking coefficient of only $(67 \pm 7) \%$ was determined for the highest laser fluence
24 of $(248 \pm 26) \text{ mJ/cm}^2$. Therefore, in order to avoid a high amount of desorbed atoms during
25 laser-assisted growth, i.e. to have optimum growth conditions, the usage of laser fluences
26 lower than 75 mJ/cm^2 is recommended.

1 **5. Conclusions**

2 We have developed a new method which allows us to model precisely the optical spectra of
3 nanoparticle ensembles and to determine their exact morphology, i.e. the equivalent radius
4 and axial ratio of single nanoparticles within the distribution.

5 The theory of quasistatic approximation was used to calculate the optical response of the
6 nanoparticles and to reproduce the extinction spectra by our model. In this way the apparent
7 distribution of axial ratios was determined which demonstrates the impact of nanoparticles
8 with a certain axial ratio within the nanoparticle ensemble on the optical spectrum. We found
9 that the optical spectra of silver and gold nanoparticle ensembles are mostly dominated by
10 very oblate nanoparticles with axial ratios of less than $x = 0.2$.

11 With our model we calculated the correlation between the axial ratio and the equivalent
12 particle radius of *single* nanoparticles in an ensemble. This functional dependence was used to
13 calculate the most probable axial ratio of the nanoparticle ensemble, i.e. the axial ratio of the
14 nanoparticles with $R_{\text{eq}} = \langle R_{\text{eq}} \rangle$. For the samples investigated in this paper values between $x =$
15 0.3 and $x = 0.5$ were found.

16 Furthermore, our model was used to determine the average equivalent radius of nanoparticle
17 ensembles where the amount of deposited material is unknown, e.g. as result of laser
18 irradiation. In this case we set the average equivalent radius as a free parameter and supplied
19 the number density of the particles on the surface and the optical spectrum as input data. We
20 were able to calculate the remaining amount of material on a substrate, i.e. after laser induced
21 desorption. We found a strong decrease of the remaining material in dependence of the laser
22 fluence and we demonstrated that for laser assisted growth with low laser fluences mostly
23 diffusion rather than desorption is dominating the process.

24

25 **Acknowledgment**

26 Financial support by the EU network "NanoCluster" under grant number HPRN-CT-2002-00,
27 by the Deutsche Forschungsgemeinschaft, SPP 1093 and by the Kasseler Hochschulbund
28 (C.H.) is gratefully acknowledged.

1 Literature

- 2 [Bauer99] G. Bauer, F. Pittner, T. Schalkhammer, *Mikrochim. Acta* **131**, 107 (1999).
- 3 [Bäumer99] M. Bäumer, H.-J. Freund, *Prog. Surf. Sci.* **61**, 127 (1999)
- 4 [Bonch01] A. M. Bonch-Bruевич, T. A. Vartanyan, N. B. Leonov, S. G. Przhibel'skii, V. V.
5 Khromov, *Optics and Spectrosc.* **91**, 779 (2001)
- 6 [Bosbach00] J. Bosbach, F. Stietz, T. Wenzel, F. Träger, Tailoring the shape of small metal
7 particles through laser irradiation during and after growth in "Cluster and Nanostructure
8 Interfaces", editors: P. Jena, B. K. Rao, S.N. Khanna, World Scientific (Singapore), 671
9 (2000)
- 10 [Bosbach02] J. Bosbach, C. Hendrich, F. Stietz, T. Vartanyan, F. Träger, *Phys. Rev. Lett.* **89**,
11 257404 (2002).
- 12 [Bohren83] C. F. Bohren, D. R. Huffman: Absorption and Scattering of Light by Small
13 Particles, Wiley, New York, 1983.
- 14 [Bowen99] W. Bouwen, E. Kunnen, K. Temst, P. Thoen, M.J. Van Bael, F. Vanhoutte, H.
15 Weidele, P. Lievens, R. E. Silverans, *Thin Solid Films* **354**, 87-92 (1999)
- 16 [Burshtain99] D. Burshtain, L. Zeiri, S. Efrima, *Langmuir* **15**, 3050-3055 (1999)
- 17 [Edward98] D. Edward, I. Palik, *Handbook of Optical Constants of Solids*, Academic Press,
18 Orlando, FL, 1995.
- 19 [Fu05] G.S.Fu, Y.L. Wang, L.Z. Chu, *Europhys. Lett.* **69**, 758-762 (2005)
- 20 [Germain05] V. Germain, A. Brioude, D. Ingert, M.P. Pileni, *J. Chem. Phys.* **122**, 124707
21 (2005)
- 22 [Grabar97] K. C. Grabar, K. R. Brown, C. D. Keating, S. J. Stranick: *Anal. Chem.* **69**, 471
23 (1997).
- 24 [Grigoriev97] I. Grigoriev, E. Meilikhov: *Handbook of Physical Quantities*, CRC Press,
25 Boca Raton, Florida, 1997.
- 26 [Hendrich03] C. Hendrich, J. Bosbach, F. Stietz, F. Hubenthal, T. Vartanyan, F. Träger, *Appl.*
27 *Phys. B* **76**, 869 (2003).
- 28 [Johnson72] P. B. Johnson, R. W. Christy, *Phys. Rev. B* **6**, 4370 (1972).
- 29 [Kreibig95] U. Kreibig, M. Vollmer: *Optical Properties of Metal Clusters*, Springer
30 Series in Material Science 25 (Springer, Berlin 1995)
- 31 [Link00] S. Link, C. Burda, B. Nikoobakht, M. A. El-Sayed, *J. Phys. Chem. B* **104**, 6152
32 (2000).
- 33 [MacDonald02] K. F. MacDonald, V. A. Fedotov, S. Pochon, K. J. Ross, G. C. Stevens, N. I.
34 Zheludev, W. S. Brocklesby, *Appl. Phys. Lett.* **80**, 1643-1645 (2002)

- 1 [Maier03] S. Maier, P.G. Kik, H.A. Atwater, S.Meltzer, E. Harel, B.E. Koel, A.A.G.
2 Requicha, Nat. Mater. **2**, 229 (2003)
- 3 [Mandal04] M. Mandal, S. Kundu, S.K. Ghosh, N.R. Jana, M. Panigrahi, T. Pal, Curr. Sci.
4 India **86**, 556-559, 2004
- 5 [Mie08] G. Mie: Beiträge zur Optik trüber Medien speziell kolloidaler Metallösungen,
6 Ann. Phys. **25**, 377 (1908)
- 7 [Ouacha05] H. Ouacha, C. Hendrich, F. Hubenthal, F. Träger, Appl. Phys. B **81**, 663 (2005)
- 8 [Pauwels00] B. Pauwels, G. Van Tendeloo, W. Bouwen, L. T. Kuhn, P. Lievens, H. Lei, M.
9 Hou, Phys. Rev. B **62**, 10383-10393 (2000)
- 10 [Press92] W. Press, S. Teukolsky, W. Vetterling, B. Flannery: Numerical Recipes in C,
11 Cambridge University Press, New York, 1992, 2. Edition
- 12 [Renteria05] V. M. Renteria, J. Garcia-Macedo, Mat. Chem. Phys. **91**, 88-93 (2005)
- 13 [Safanov98] V. P. Safonov, V. M. Shalaev, V. A. Markel, Y. E. Danilova, N. N. Lepeshkin,
14 W. Kim, S. G. Rautian, R. L. Armstrong, Phys. Rev. Lett. **80**, 1102 (1998).
- 15 [Sugiyama04] M. Sugiyama, G. Sigesato, J. Electron Microsc. **53** (5): 527-536 (2004)
- 16 [Stietz01] F. Stietz: Appl. Phys. A. **72**, 381 (2001)
- 17 [Vartanyan01] T. Vartanyan, J. Bosbach, F. Stietz, F. Träger, Appl. Phys. B **73**, 291 (2001).
- 18 [Vartanyan02] T. Vartanyan, J. Bosbach, C. Hendrich, F. Stietz, F. Träger, Proc. SPIE **4636**,
19 31 (2002),
- 20 [Wakayama99] Y. Wakayama, S. Tanaka, Surf. Sci. **420**, 190 (1999)
- 21 [Wenzel99] T. Wenzel, J. Bosbach, F. Stietz, F. Träger: Surf. Sci. **432**, 257 (1999)
- 22 [Wenzel99a] T. Wenzel, J. Bosbach, A. Goldmann, F. Stietz, F. Träger, Appl. Phys. B **69**, 513
23 (1999).
- 24 [Winterbottom67] W. L. Winterbottom: Acta Metal. **15**, 303 (1967)
- 25 [Xu05] G. Xu, M. Tazawa, P. Jin, S. Nakao, Appl. Phys. A **80**, 1535-1540 (2005)
- 26 [Yamaguchi74] T. Yamaguchi, S. Yoshida, A. Kinbara, Thin Solid Films **21**,
27 173 (1974).
- 28 [Ziegler04] T. Ziegler, C. Hendrich, F. Hubenthal, T. Vartanyan, F. Träger, Chem. Phys. Lett.
29 **386**, 319 (2004).

1 Figures

2

3 **Fig. 1: a)** Extinction spectrum of silver nanoparticles with $\langle R_{\text{eq}} \rangle = 8.3$ nm on sapphire
4 (squares) and the corresponding result of a fit of Eq. (5) (solid line), **b)** apparent axial ratio
5 distribution $f_{\text{ab}}(x)V(x)$, **c)** experimental data (squares) and the resulting spectrum from the
6 modeling with Eq. (12) (solid line), **d)** relationship between axial ratio x and equivalent radius
7 R_{eq} of the particles within the ensemble (solid line) and the frequency distribution of the radii
8 of the particles in arbitrary units (dashed line).

9

10 **Fig. 2: a)** Extinction spectrum of silver nanoparticles on TiO_2 for an effective coverage of 3.3
11 nm (from [Xu05], squares) and the corresponding fit with Eq. (5) (solid line), **b)** apparent
12 axial ratio distribution, **c)** experimental data (squares) and resulting spectrum from the
13 modeling with Eq. (12) (dashed line: $\langle R_{\text{eq}} \rangle = 8.9$ nm, solid line: $\langle R_{\text{eq}} \rangle = 6.9$ nm), **d)**
14 relationship between axial ratio x and equivalent radius R_{eq} of the particles within the
15 ensemble (solid line) and the frequency distribution of the radii of the particles in arbitrary
16 units (dashed line)

17

18 **Fig. 3: a)** Extinction spectrum of gold nanoparticles with $\langle R_{\text{eq}} \rangle = 6.3$ nm on sapphire
19 (squares) and the corresponding fit with Eq. (5) (solid line), **b)** apparent axial ratio
20 distribution, **c)** experimental data (squares) and resulting spectrum from the modeling with
21 Eq. (12) (solid line), **d)** relationship between axial ratio x and equivalent radius R_{eq} of the
22 particles within the ensemble (solid line) and the frequency distribution of the radii of the
23 particles in arbitrary units (dashed line)

24

25 **Fig. 4: a)** Extinction spectra of an ensemble of gold nanoparticles with $\langle R_{\text{eq}} \rangle = 6.3$ nm on
26 sapphire before (black squares) and after spectral hole burning (open squares) with laser light
27 of a photon energy of 1.65 eV (dashed line). The solid curves correspond to the modeled
28 spectra from Eq. (5). **b)** The apparent axial ratio distribution before (solid line) and after hole
29 burning (dashed line). The cross-section of the laser light is located at an axial ratio of $x =$
30 0.09.

31

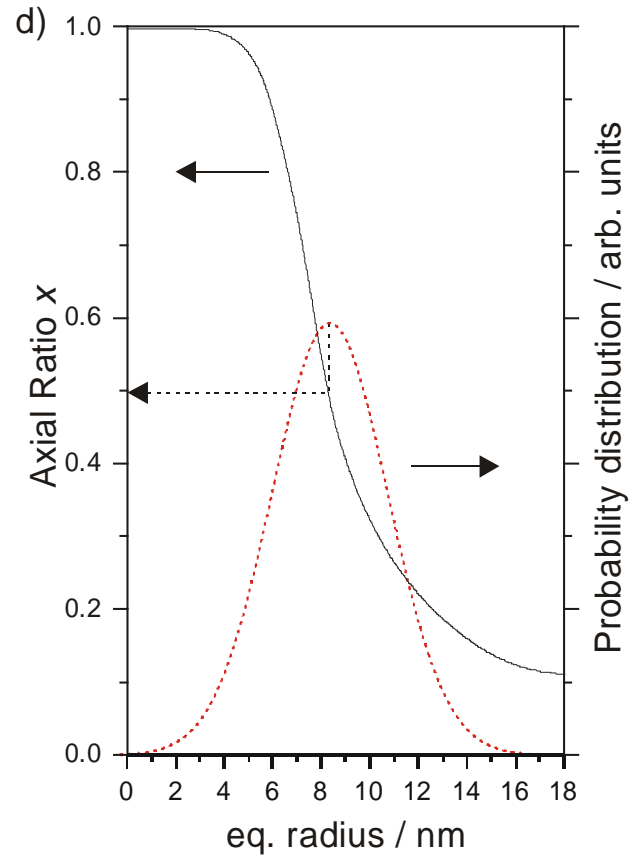
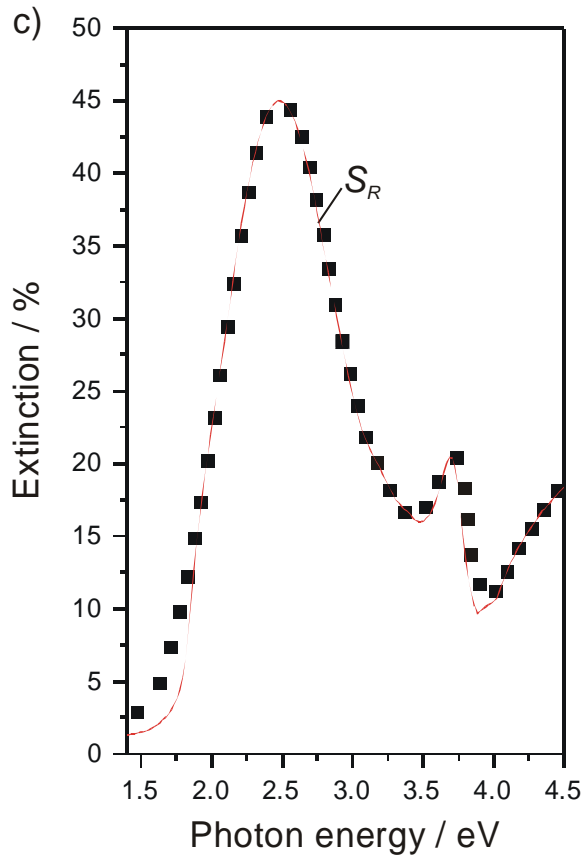
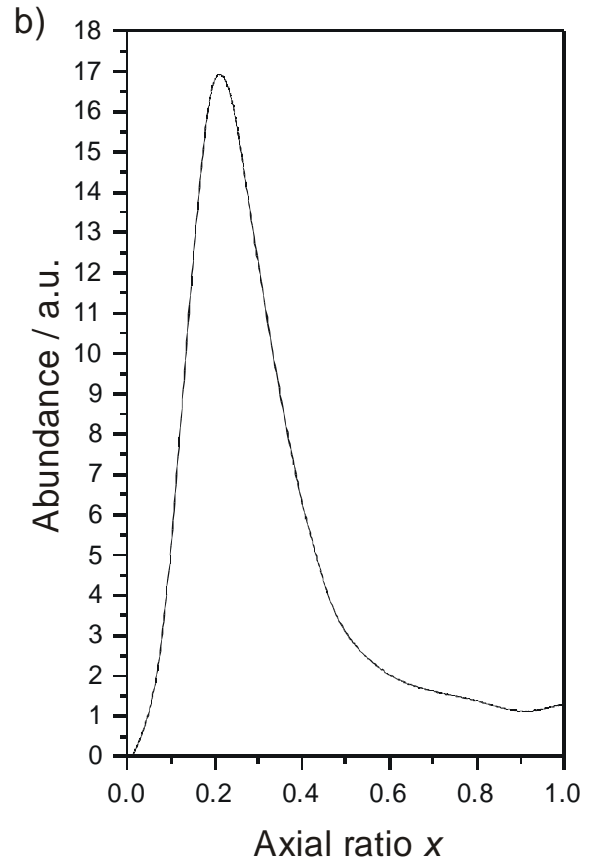
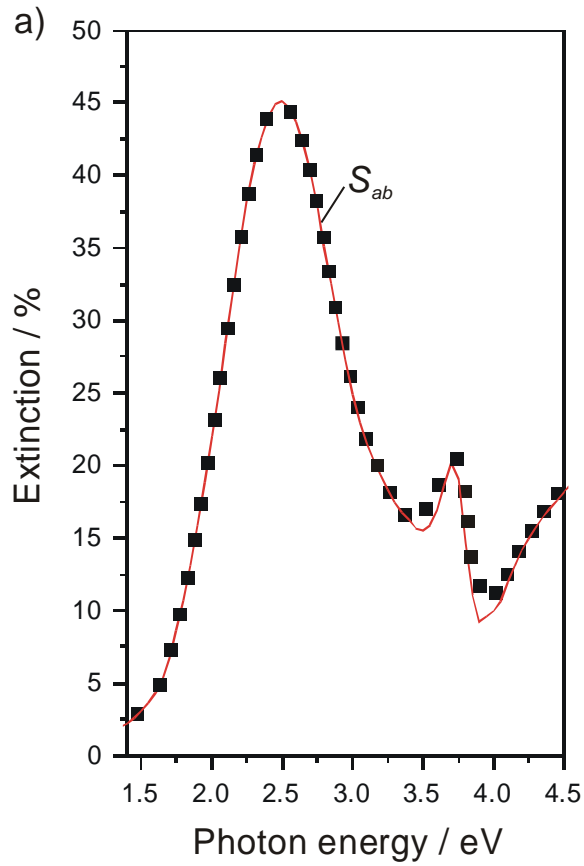
32 **Fig. 5: a)** Extinction spectrum of gold nanoparticles on sapphire prepared by laser-assisted
33 growth (squares) and the modeled curve from a fit with Eq. (5) (solid line). The vertical line
34 indicates the photon energy of the laser light. **b)** Apparent axial ratio distribution for a

1 nanoparticle ensemble prepared with laser assisted growth. The axial ratio of the particles
2 which are resonant with the laser light is marked with the vertical solid line.

3

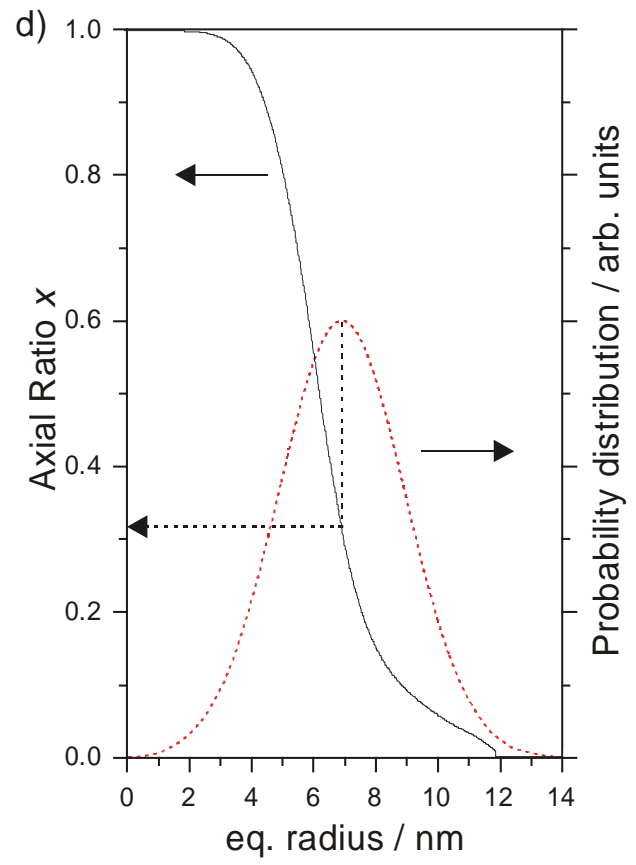
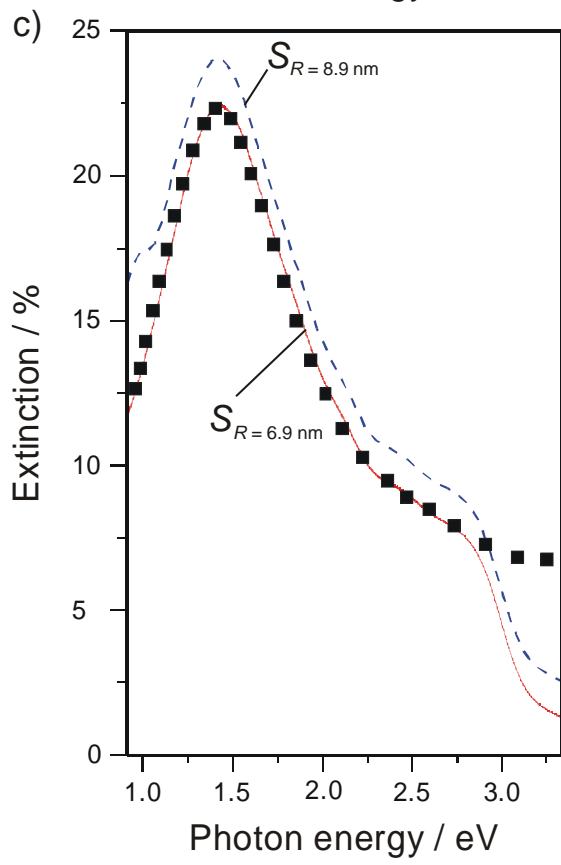
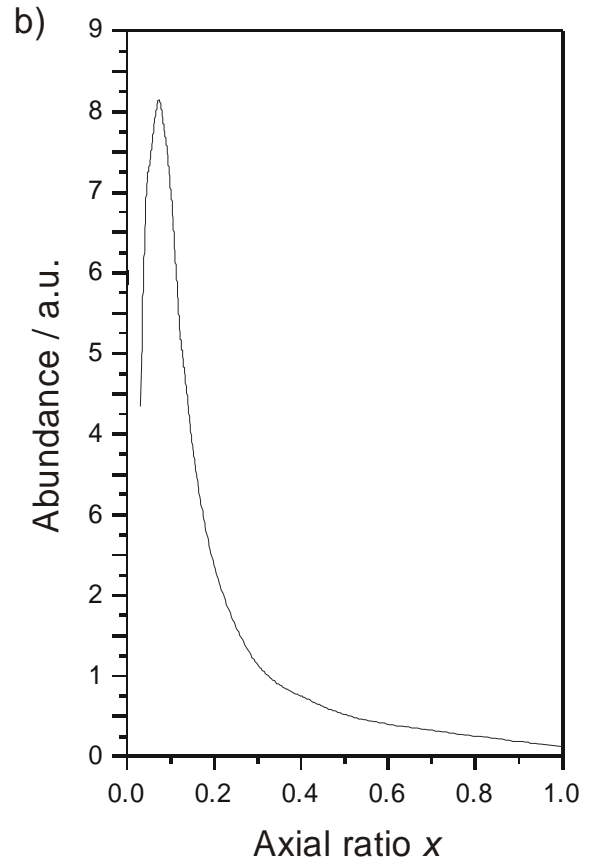
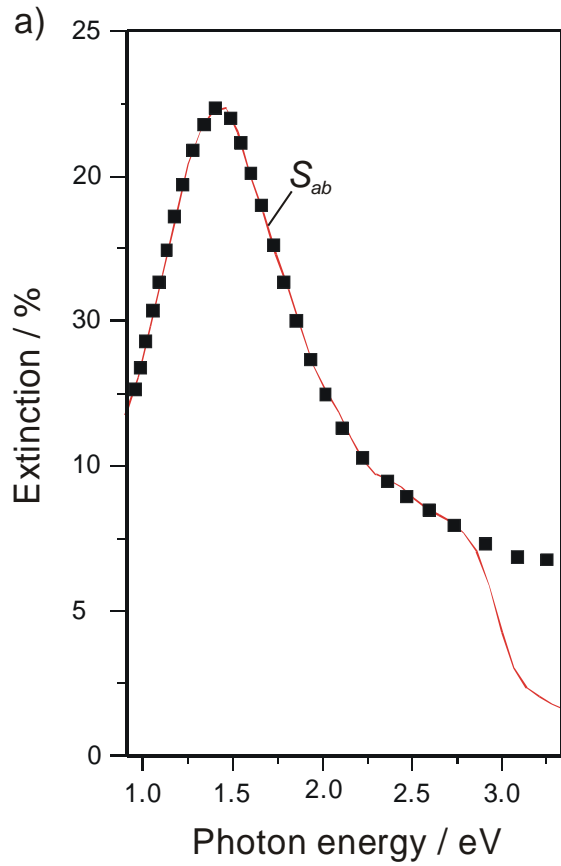
4 **Fig. 6:** Effective sticking coefficients of gold atoms on sapphire during laser-assisted growth
5 as function of the laser fluence. The values are calculated from the extinction spectra of
6 nanoparticle ensembles prepared with laser-assisted growth by using a photon energy of 1.65
7 eV. A sticking coefficient of 100% corresponds to $5.6 \cdot 10^{16}$ atoms/cm² on the sample. The
8 solid line is a guide to the eye.

1 Fig. 1



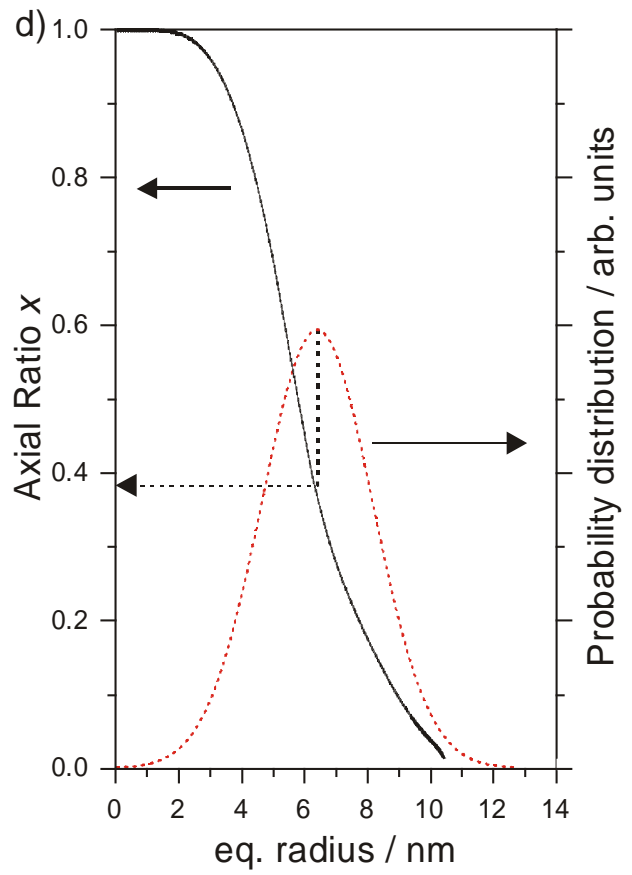
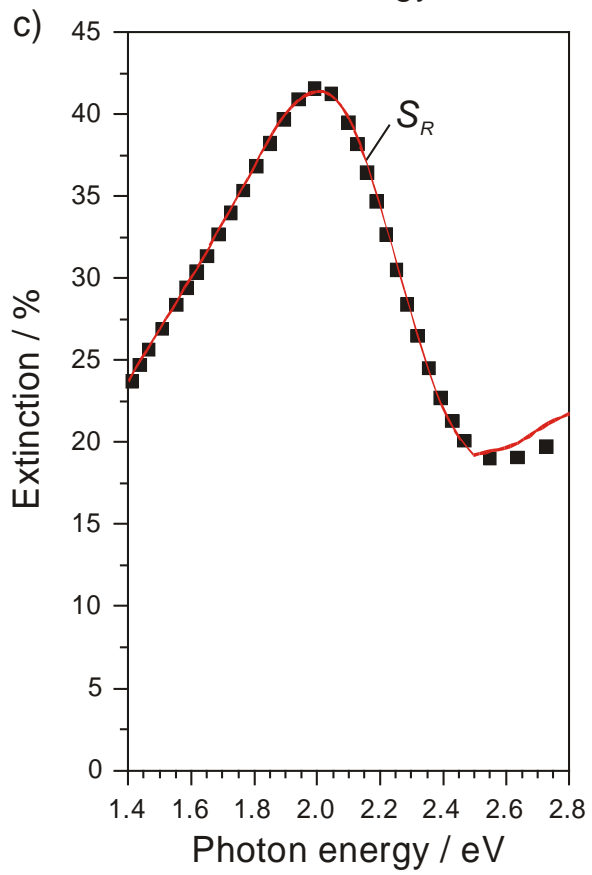
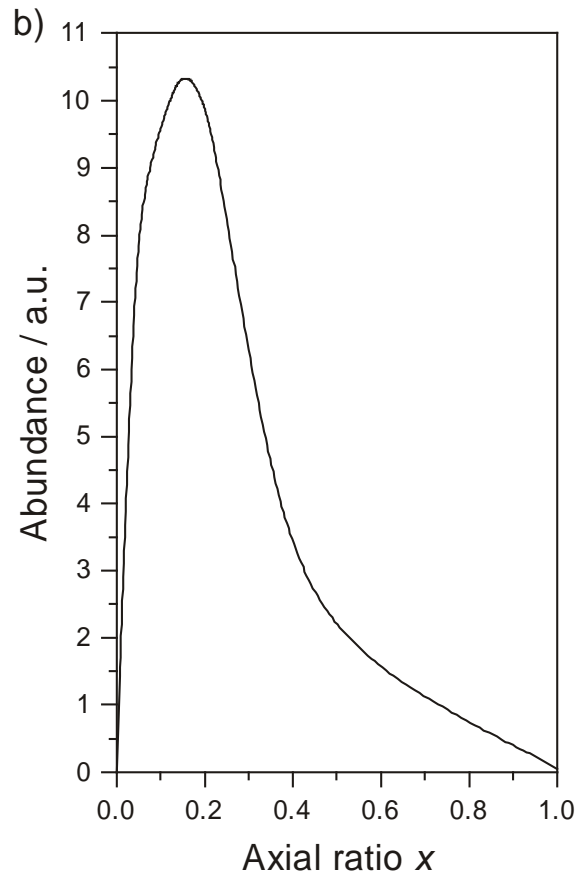
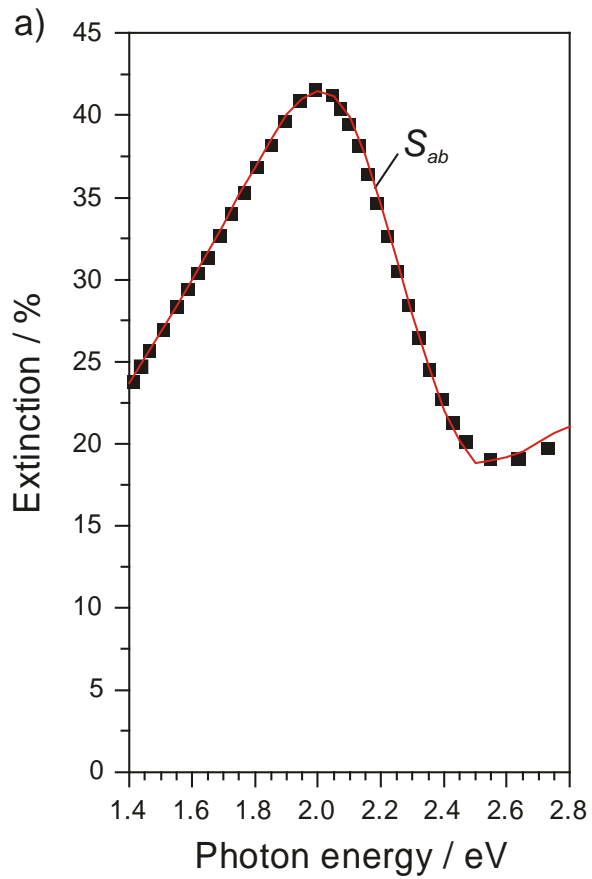
2
3

1 Fig. 2



2
3

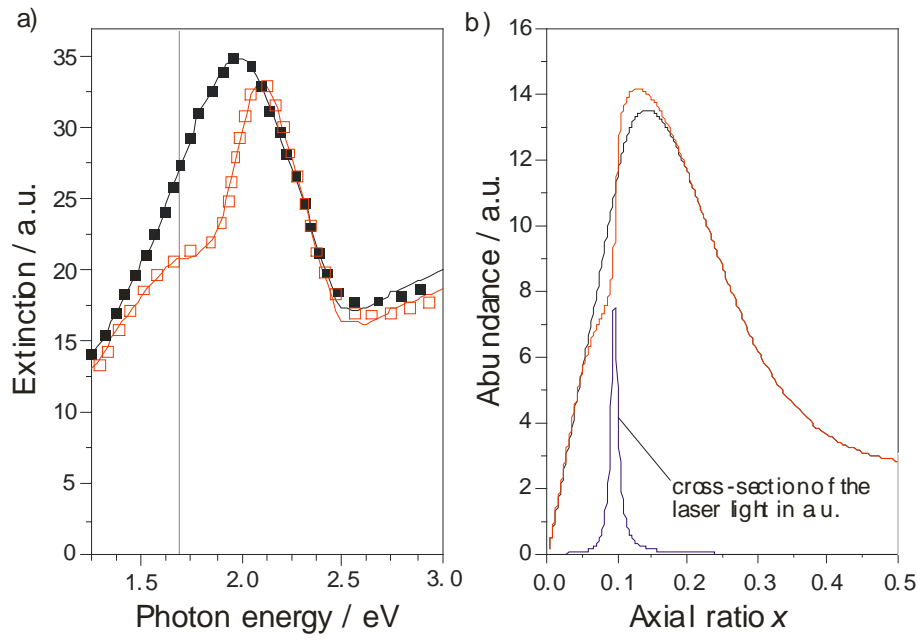
1 Fig. 3



2
3

1 Fig. 4

2



3

4

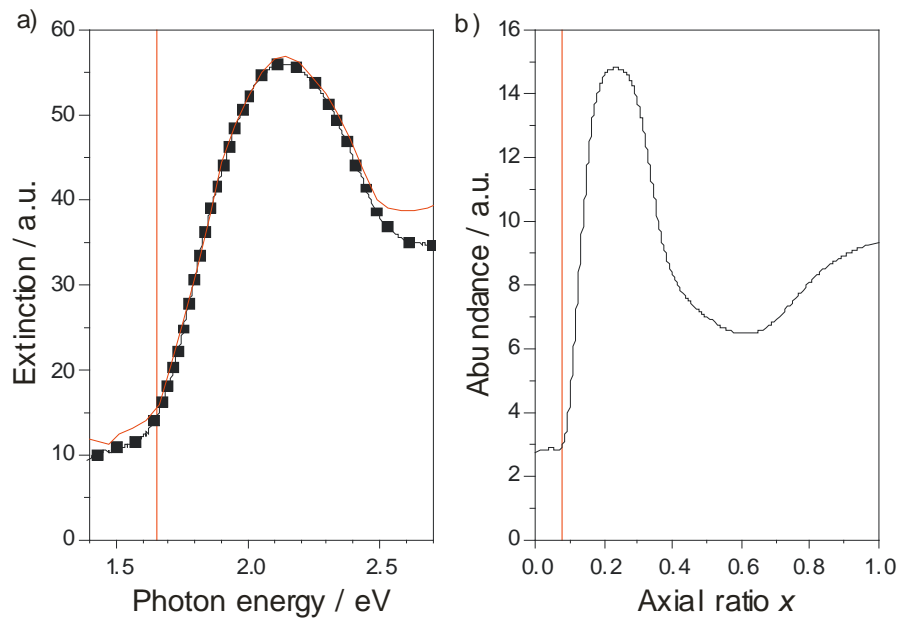
5

6

7

8 Fig. 5

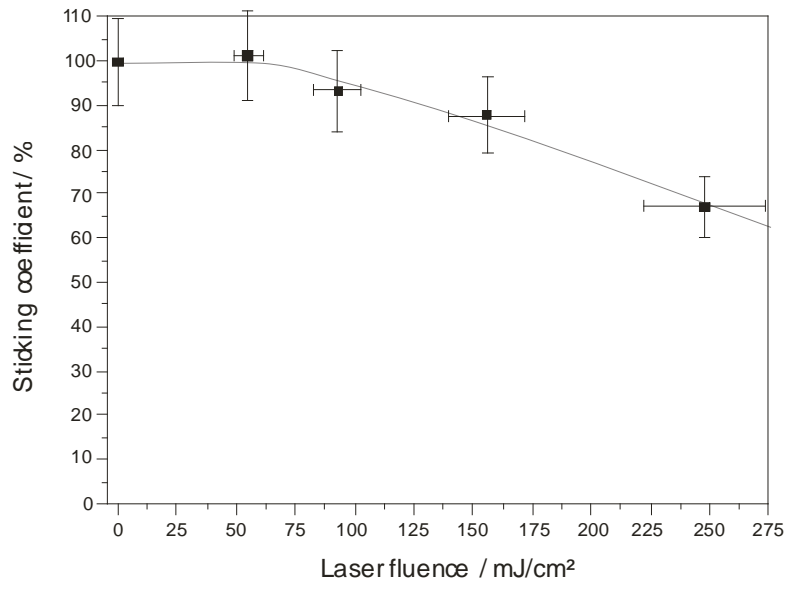
9



10

1 Fig. 6

2



3